SANDIA REPORT

SAND2012-7770
Unlimited Release
Printed September and 2012

Epsilon Near Zero Material for Electromagnetic Energy Transport through Sub-wavelength Channels

Ganapathi Subramania, Arthur J. Fischer, Ting S. Luk and I. Brener

Prepared by
Sandia National Laboratories
Albuquerque, New Mexico 87185 and Livermore, California 94550

Sandia National Laboratories is a multi-program laboratory managed and operated by Sandia Corporation, a wholly owned subsidiary of Lockheed Martin Corporation, for the U.S. Department of Energy's National Nuclear Security Administration under contract DE-AC04-94AL85000.

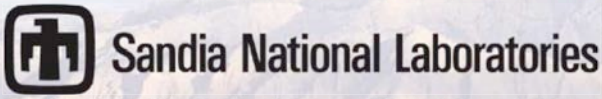

Issued by Sandia National Laboratories, operated for the United States Department of Energy by Sandia Corporation.

Available to DOE and DOE contractors from
U.S. Department of Energy
Office of Scientific and Technical Information
P.O. Box 62
Oak Ridge, TN 37831

Telephone: (865) 576-8401
Facsimile: (865) 576-5728
E-Mail: reports@adonis.osti.gov
Online ordering: http://www.osti.gov/bridge

Available to the public from
U.S. Department of Commerce
National Technical Information Service
5285 Port Royal Rd.
Springfield, VA 22161

Telephone: (800) 553-6847
Facsimile: (703) 605-6900
E-Mail: orders@ntis.fedworld.gov
Online order: http://www.ntis.gov/help/ordermethods.asp?loc=7-4-0#online

SAND2012-7770
Unlimited Release
Printed September 2012

Epsilon Near Zero Material for Electromagnetic Energy Transport through Sub-wavelength Channels

Ganapathi Subramania
Advanced Material Sciences

Arthur J. Fischer
Semiconductor Materials and Device Sciences

Ting S. Luk
Nanostructure Physics

Igal Brener
Applied Photonic Microsystems

Sandia National Laboratories
P.O. Box 5800
Albuquerque, New Mexico 87185-MS1082

Abstract

Efficient transport of electromagnetic energy through subwavelength channels in the optical regime can dramatically enhance the performance of subwavelength imaging, photovoltaics, sensing and light emission. Epsilon Near Zero (ENZ) materials can be artificially created and tailored to have near-zero dielectric constant at a desired wavelength and have the potential to achieve sub-wavelength energy transport. This report describes the fabrication of ENZ at visible frequencies from a multilayer composite of silver and titanium oxide and the evaluation of its optical properties. An approach based on nanpatterned double-grooved, periodic metal film structure for achieving broadband subwavengths energy transport is also discussed. Such as system enable light confinement to an area $(\lambda/250)^2$ at mid infrared wavelengths.

ACKNOWLEDGMENTS

Authors would like to acknowledge Travis Young and Carlos Sanchez for film deposition aspect during the fabrication of the ENZ and double groove samples. This work was performed, in part, at the Center for Integrated Nanotechnologies, a U.S. Department of Energy, Office of Basic Energy Sciences user facility. Sandia National Laboratories is a multi-program laboratory managed and operated by Sandia Corporation, a wholly owned subsidiary of Lockheed Martin Corporation, for the U.S. Department of Energy's National Nuclear Security Administration under contract DE-AC04-94AL85000.

CONTENTS

FIGURES

NOMENCLATURE

dB	decibel
UV	ultraviolet
IR	Infrared
DG	Double-grooved
PCF	Power confinement factor
EOT	Extra-ordinary Optical Transmission

1. INTRODUCTION

Confining and enhancing light within deep subwavelength volumes is key to the enhancement of light-matter interaction with great implications in the control of absorption and emission rates, as well as in attaining high optical nonlinearities and/or gain. Efficient transport of electromagnetic energy through subwavelength channels in the optical regime can dramatically enhance the performance of subwavelength imaging, photovoltaics, sensing and light emission. Current approaches based on plasmonic structures or negative index metamaterials tend to be lossy due to material absorption and have a small bandwidth due to reliance on resonance behavior. Recently, epsilon-near-zero (ENZ) material has been proposed as a way to achieve efficient subwavelength electromagnetic energy transport. ENZ materials have near-zero dielectric constant (epsilon) in the effective medium limit resulting in an unusually large effective wavelength even at optical frequencies is thus expected to enable energy squeezing and transfer through subwavelength channels with lower losses over larger bandwidth. The optical properties of materials which is the response to an applied external electromagnetic field can be expressed using the relative permittivity(ε) and the relative permeability(μ) of the medium.

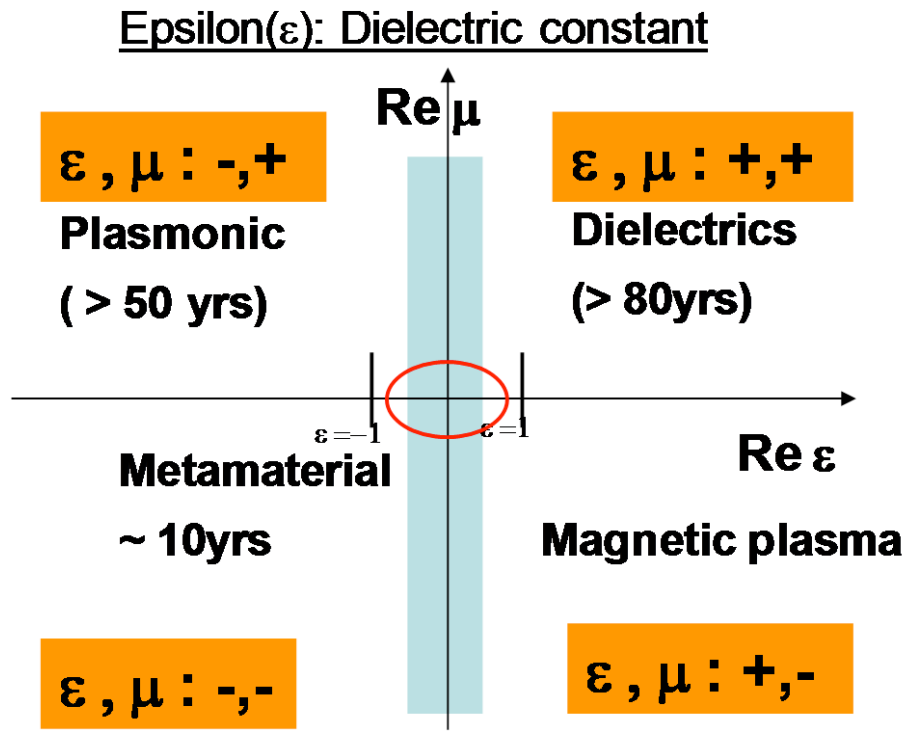

Figure 1: Epsilon(ε) / Mu(μ) map showing classification of material based on its electromagnetic response.

One possible way to classify optical materials is based on where they lie in the re(ε), re(μ) map (Figure 1). For instance, most dielectric materials lie on the first quadrant (re(ε,μ) > 0) while metals lie in the second quadrant (re(ε)<0 re(μ) > 0)., In the recent years, there has been an extraordinary interest in negative index materials (re(ε,μ) < 0 : 3rd quadrant) and magnetic plasma materials (re(ε)<0 re(μ) > 0: 4th quandrant) that typically do not occur naturally. Such

artificial materials encompass a broad area known as 'metamaterials'. However more recently, another region of the re(ε,μ) map that lies near the origin i.e. $\varepsilon,\mu \sim 0$ has attracted attention. Of particular interest is the $|\varepsilon| \sim 0$ region compared to $|\mu| \sim 0$, as $|\varepsilon| \sim 0$ is more easily achieved in practice using metals whose dielectric constant passes through zero (at the plasma frequency). In this regime refered to as "epsilon near zero" (ENZ), the electric field displacement(**D**) which is related to the electric field (**E**) as $\mathbf{D}=\varepsilon\mathbf{E}$ also approaches zero, causing the phase velocity of electromagnetic waves through the medium to diverge, implying diverging wavelength. This is a unique property that can lead to near zero frequency behavior (direct current) at optical frequencies.

ENZ material has been shown theoretically[1] and in recent experiments at microwave frequencies[2,3] to be an excellent candidate for energy transport through subwavelength channels. At optical frequencies ENZ materials would represent the leading edge of metamaterials research with potential to revolutionize many areas such as subdiffraction imaging, cloaking, sensing, light emission and photovoltaics. But most importantly, the extraordinary property of ENZ material of vanishing displacement field and diverging phase velocity makes it uniquely suitable as building blocks for optical nanocircuitry[4] that can potentially overcome Moore's law limitations. In this report we discuss our work on the fabrication of ENZ mematerial as an effective medium composite using a metal-dielectric multilayer stack operating at visible frequencies. In section two we will discuss the optical properties of the Ag/TiO_2 multilayer composite and evaluate the effect of metal losses on the ENZ behavior of this structure.

In section three we will theoretically explore an approach that utilizes of the metal nanostructures at optical frequencies to achieve ultra-subwavelength light confinement down to $(\lambda/250)^2$ while simultaneously achieving a large electric field enhancement. Futhermore disproportionately large amount of the incoming electromagnetic power can be funneled into the small area. This behavior is broadband, covering a wavelength region of 3-20 μm. This approach does not rely on ENZ metamaterials or surface plasmon excitation in metals but relies on an inherently non-resonant process of quasistatic excitation of charges in the metal. This design is amenable to nanofabrication techniques and can have significant impact on light matter interaction for enhancement of photonic density of states, non-linearity, absorption efficiency and energy conversion.

2. ENZ METAMATERIAL FROM METAL-DIELECTRIC COMPOSITE AT OPTICAL FREQUENCIES

ENZ metamaterial can be achieved using a composite structure that can possess an effective vanishing dielectric constant. Such a structure is more suitable for creating channels forming optical connecting 'wires' that can be utilized for optical nanocircuits[4]. While metals by themselves can be ENZ material their scope is limited. Metals have a negative dielectric constant for most of the frequency range and their dielectric response [$\varepsilon(\omega)$] as a function of frequency 'ω' for most practical purposes are well described by the Drude model

$$\varepsilon(\omega) = 1 - \frac{\omega_p^2}{\omega^2 + i\gamma\omega} \quad \text{--- (1),}$$

At high enough frequency such as that approaching ω_p the damping loss term is small enough and $\varepsilon(\omega) \sim 0$. Since ω_p is fixed for a given metal, we can achieve $\varepsilon(\omega) \sim 0$ only for at limited set of frequencies that are typically in the UV. However, we can lift this restriction by fashioning a material that is a composite of $\varepsilon(\omega) < 0$ (e.g. metals) and $\varepsilon(\omega) > 0$ (e.g. dielectrics). In theory, by appropriately combining metals and dielectrics one might be able to create an ENZ material operating at a frequency of one's choice. The optical properties of a composite medium in three dimensions such as the metal-dielectric composite can be described in the long wavelength limit by effective medium theory[5] (EMT). Effective medium theory (EMT) can be used to design metal-dielectric composites in one, two and three dimensions to achieve required effective dielectric parameters. The common EMT used to describe optical properties of a composite material where a smaller fraction(f) of one material (ε_1) typically spherical inclusions, is embedded inside a host material (ε_h) is the Maxwell-Garnet theory (MGT)[5] which gives a reasonable estimation of the dielectric constant given by

$$\varepsilon = \varepsilon_h + 3f\varepsilon_h \frac{\varepsilon_1 - \varepsilon_h}{\varepsilon_1 + 2\varepsilon_h} + O(f^2) \quad \text{---(2).}$$

This is a special case of a more general effective medium expression developed by Bruggeman[5] for composite media with multiple components with fraction (f_i) given by

$$\sum_i f_i \frac{\varepsilon_i - \varepsilon}{\varepsilon_i + 2\varepsilon} = 0, \quad \sum_i f_i = 1 \quad \text{---(3).}$$

Ideally, a three-dimensional architecture of metal-dielectric composite can result in an ENZ material that offers the largest degree of freedom but it is considerably harder to implement. Due to the limited scope of this single investigator project and to mitigate some of the technical challenges, we decided to investigate a one-dimensional(1D) architecture consisting of alternating layers of metal and dielectric of subwavelength thickness (Figure 1). This is simpler to implement and has been widely studied for various other applications including negative index metamaterials[6,7]. It should be noted that despite the reduced degree of freedom offered by the 1D approach we can still obtain valuable insight into the light propagation in the ENZ medium that can be applied in the future to extend to higher dimensions. In the 1D case, the effective medium

behavior can be obtained through a simple analysis[8]. This structure is anisotropic possessing two different dielectric constants[9] one for the electric field polarized parallel and the other perpendicular to the metal film (Figure 1). For light incident from the top with electric field (**E**) polarized along the stack planes, boundary conditions at the interface implies continuity of **E** as it is tangential. We can therefore consider the average displacement field $\mathbf{D_{av}}$, to obtain the following:

$$D_{av} = f_m D_m + f_d D_d = f_m \varepsilon_m E_m + f_d \varepsilon_d E_d = (f_m \varepsilon_m + f_d \varepsilon_d) E = \varepsilon_{eff} E \quad \text{--- (4)}$$

where the subscripts 'm' and 'd' refer to metal and dielectric respectively. This expression enables us to choose a metal / dielectric combination in a straightforward manner based on the desired frequency of operation.

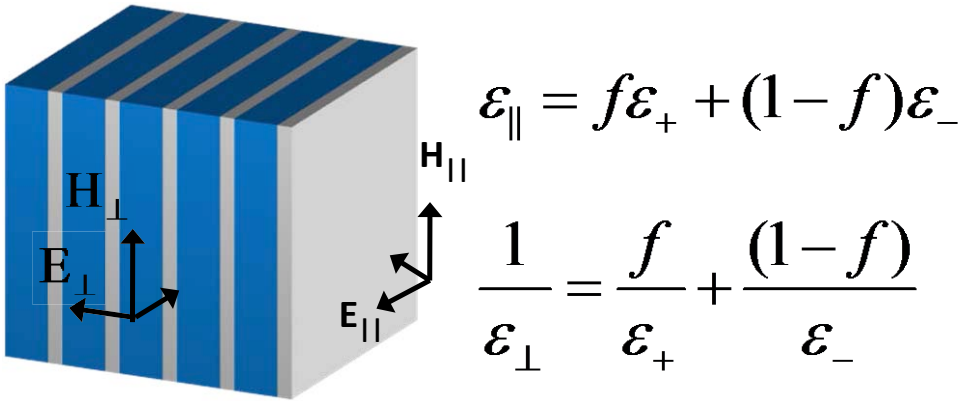

Figure 2 :Schematic of metal dielctric composite showing effective medium response for light polarized parallel and per pendicular to the film. The grey region corresponds to metal and the blue region to the dielectric.

Here we fabricate and study the optical properties of a metal-dielectric multilayer composite composed of alternating layers of silver(Ag) and titanium dioxide(TiO_2) with an effective ENZ property at visible wavelengths. Ag was chosen for the negative component of the dielectric constant due to its low imaginary part[10] ($\varepsilon_i < 2.5$) through the visible region. Oxide dielectrics such as SiO_2 and TiO_2 are potential materials for the positive component as they are non-absorbing in the visible regime. We performed finite difference time domain (FDTD) simulations on multilayer structures based both on Ag/ SiO_2 as well as Ag/ TiO_2 composites to determine the most optimal design for fabrication which show interesting features. To obtain at ENZ wavelength of ~ 660 nm for light polarized along the film plane perpendicular to the film stack) we can calculate from equation (4) the composition for Ag/ SiO_2 and Ag/ TiO_2 to be 11%/89% and 23%/77% (Figure 2 and b). EMT theories typically assume small field fluctuations on the wavelength scales of interest requiring the constituent materials to be extremely sub-wavelength in thickness. For visible frequency operation the metals which have large negative values of dielectric constants needs to be of nanoscale dimensions thus, posing fabrication challenges. Therefore, due to constraints imposed by film deposition techniques on achieving

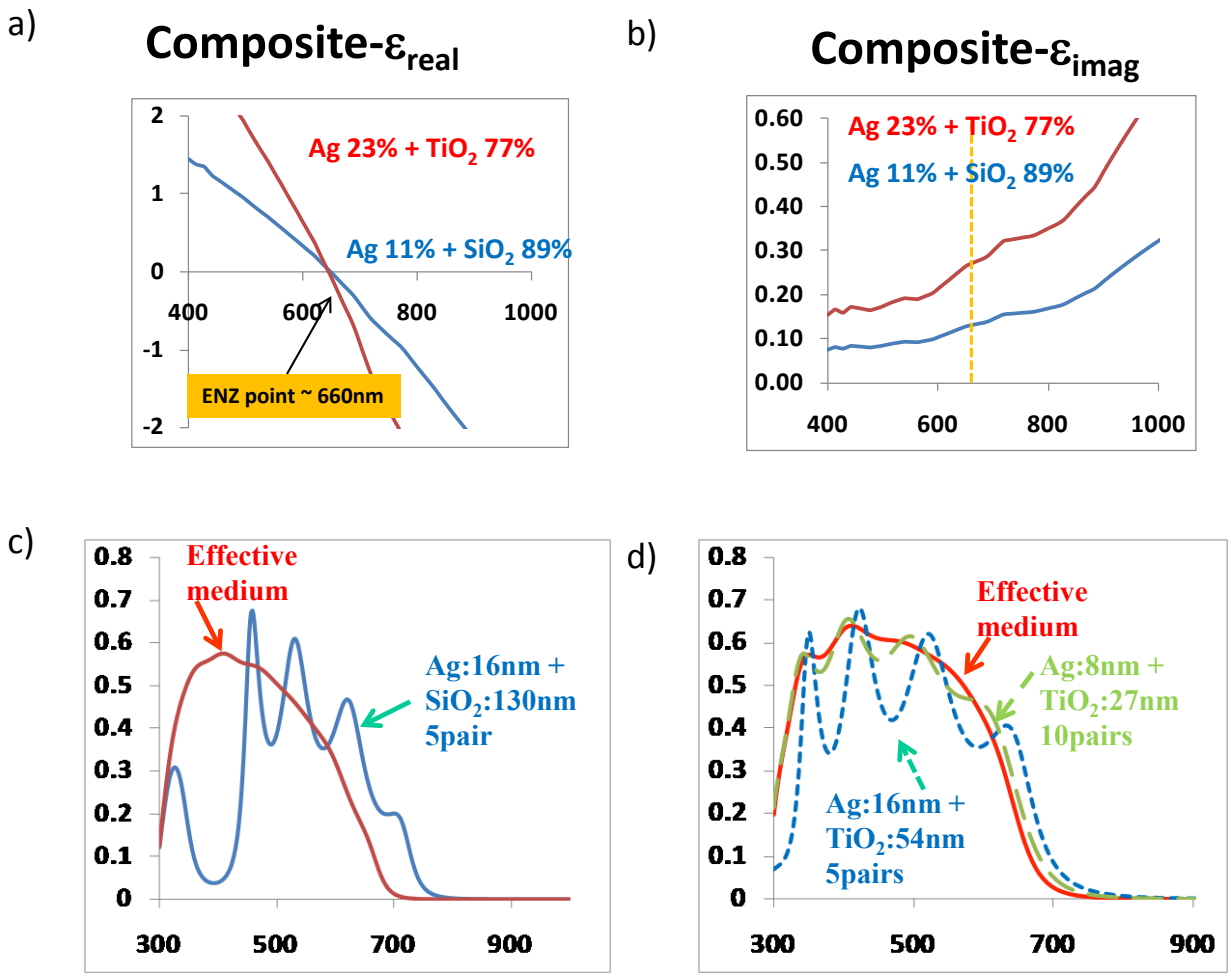

Figure 3: a) Real part of dielectric constant (ε_r) for the composite structures indicating the ENZ wavelength. b) Imaginary part of dielctric constant (ε_i) for the composite structures. c) Finite difference time domain simulation of transmission through a 5 pair composite of Ag (16nm)/SiO2 (130nm)compared to an equivalent effective medium for ENZ near 660nm. d) Finite difference time domain simulation showing transmission through a 5 pair composite of Ag(16nm)/TiO2(54nm) , 10 pair of Ag(8nm)/TiO2(27nm) compared to an equivalent effective medium for ENZ near 660nm.

thickness uniformity Ag film thickness was set to be 16nm. This results in a thickness of SiO_2 and TiO_2 of 130nm and 54nm respectively. The smaller fraction of Ag in the composite would have made it more attractive as it would have minimal losses(Figure 3b). Nonetheless, FDTD simulation (Figure 3c and d) for a 5-pair structure for both cases compared with and equivalent thickness of homogenous effective medium revealed that the spectral agreement was far better for the case of Ag/ TiO_2. The reason for this is likely due to the fact that near a wavelength of 660nm, 130nm of SiO2 corresponds to ~0.28λ_{SiO2} whereas 54nm of TiO_2 is ~0.19 λ_{TiO2} allowing for a more uniform field distribution in the latter case than the former. The importance of the field homogenization effect is also seen from the significant reduction in the oscillating features in the transmission plot for a 10pair (8nm/27nm) sample. We fabricated 4, 5 and 9 pairs

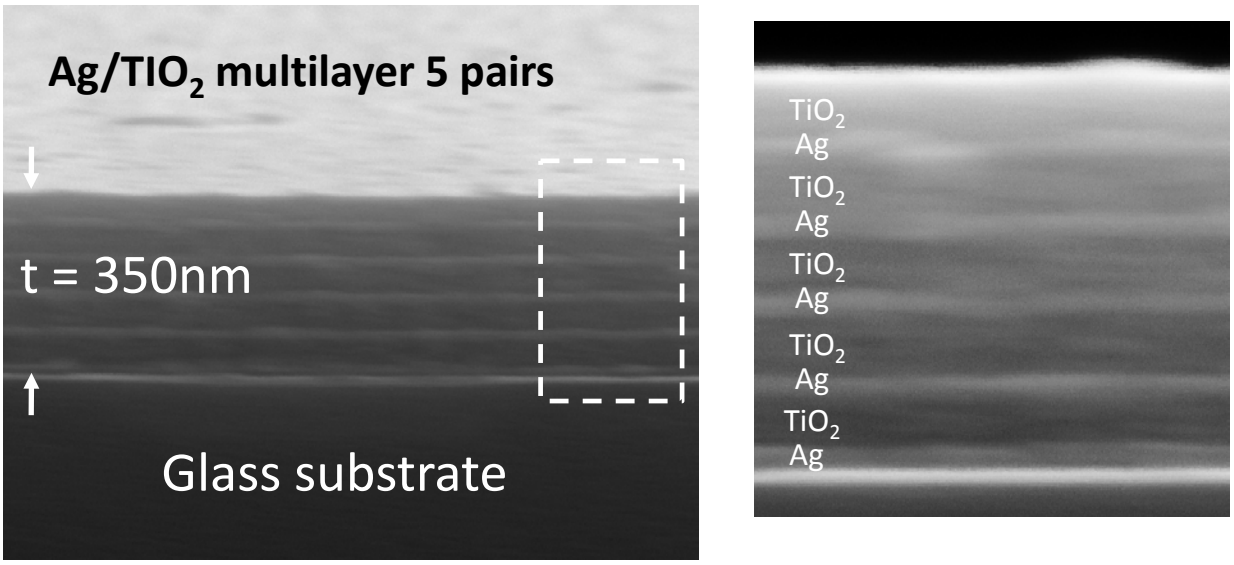

Figure 4: Cross-section scanning electron microscope(SEM) image of 5 pairs of Ag/ TiO_2 structures with a total thickness of ~ 350nm with each pair composed of ~ 16nm Ag and 54nm TiO_2 fabricated on top of a glass substrate. The right hand side image shows higher magnification image of the area in the dotted square. The alternating bright and dark bands correspond to Ag and TiO_2 layers respectively.

of Ag/ TiO_2 (16nm/54nm) using electron beam evaporation depositing alternatingly, Ag and TiO_2 films on a glass substrate starting with Ag. This enables TiO_2 to be the topmost layer thus protecting Ag from being exposed to air after fabrication and preventing it from oxidizing. The cross-section SEM images (Figure 4) clearly reveal the alternating layers and the thicknesses appear to be within 10%. Visual inspection of the films also reveal that most of the area to be of uniform color. We performed normal incidence transmission and reflectance spectroscopy on these samples. The transmission near the designed ENZ wavelength of 660nm for 4pair, 5pairs is only about 6%, and 3% respectively while for 9 pairs the transmission drops to ~0.05% (Figure 5a). These are lower than the corresponding expected values obtained from FDTD simulations (Figure 5c)values are over 35% for 4 and 5 pairs at 660nm and over 63% for 9 pairs (Figure 5b). The corresponding simulation values (Figure 5d) are closer. The oscillations in the experimental data are also suppressed relative to the simulations. Nonetheless, the maximum experimental transmission values are within a few percent of the simulation values. Certain discrepancies are to be expected due potential difference between actual layer thickness values and those used in simulations which are evident from the higher magnification cross-section image (Figure 4). As a result the ENZ wavelength position could be slightly blue or red shifted. Although the actual transmission values close to the ENZ wavelength is quite low, the transmission does improve for shorter wavelengths where the real part of dielectric constant is still less than unity. This could potentially enable a higher displacement vector (**D**) field in air leading to interesting effects. Although the effective imaginary component of the dielectric constant for this composite is only around 0.25 in this wavelength region, the low value of the real part keeps the figure-of-merit quite low. Therefore, the absorption effects are magnified.

We explored possibilities for further reducing the effective imaginary part of the ENZ composite and to boost transmission. One approach is to create a subwavelength grating

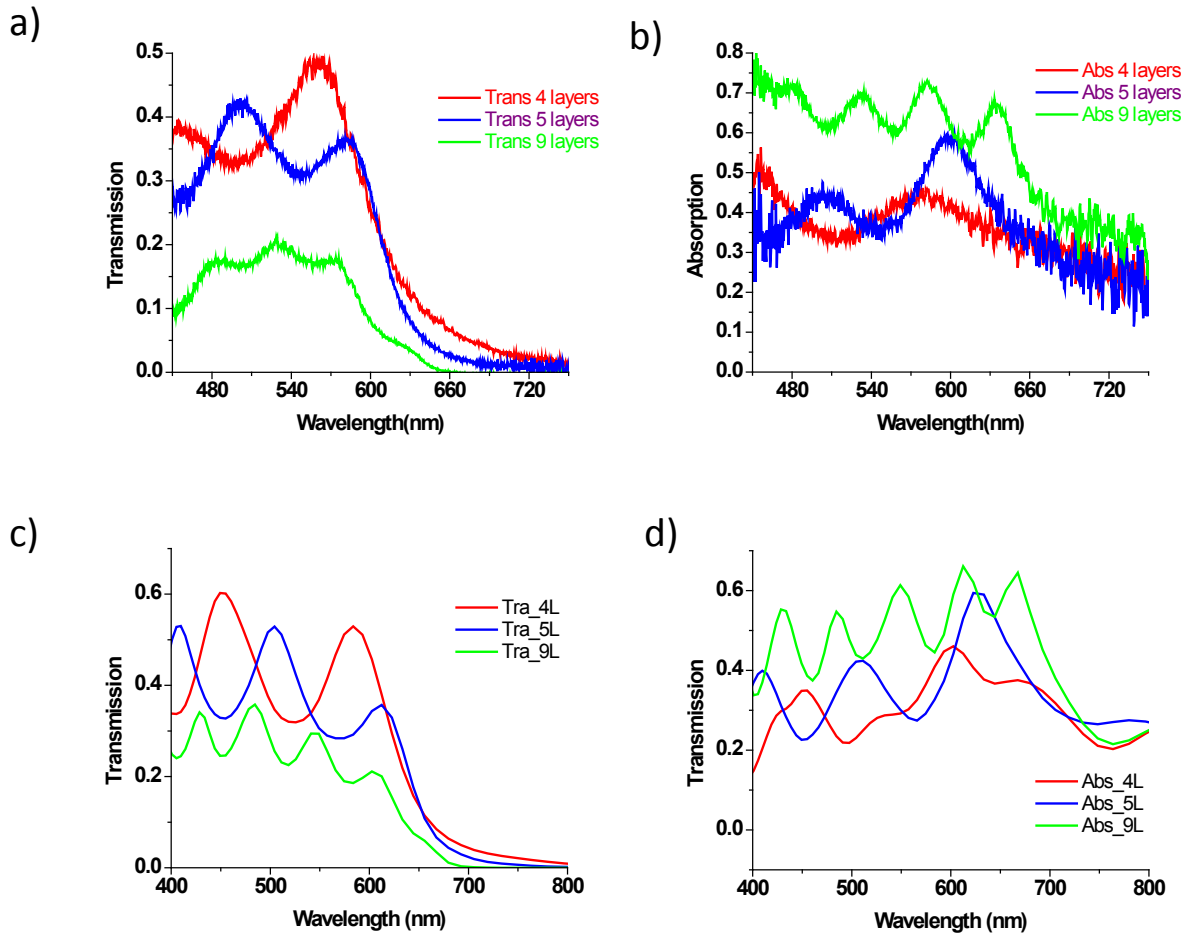

Figure 5: a) Optical transmission response at near normal incidence for 4, 5 and 9 pairs of Ag/TiO_2 structure. b) The corresponding absorption spectrum. c) Finite difference time domain simulation (Lumerical ®) of the transmission through 4, 5 and 9 pairs. d) Simulated absorption spectra for these cases.

structure. Smallest possible grating period would be ideal to obtain a nearly homogenous structure. While the multilayer structure would exhibit ENZ for normal incidence as long the electric field was polarized parallel to the film, the grating introduces additional anisotropy. Now, the electric field needs to be polarized parallel to the grating (Figure 6a) to obtain ENZ. We considered a grating period of 100 nm that is less than $\lambda/5$ and simulated transmission for 3 different grating widths of 30%, 50% and 70% of the periods. Figure 6c and d show the transmission and absorption for these different gratings compared with multilayer layer structure. For simplicity we have used an effective medium instead of the multilayer for the grating. As expected the transmission increases as the grating width is reduces by 20% at high frequencies to about 50% at the edges. It is to be noted that the creation of a grating shifts the ENZ point to longer wavelengths (Figure 6b). The transmission increases to ~ 17% for the 50% grating at the ENZ point of 725nm and then falls off to 9% at 800nm for 30% grating. The reduction in the transmission is likely due to increase in the imaginary part of the dielectric constant of the grating lines at longer wavelengths.

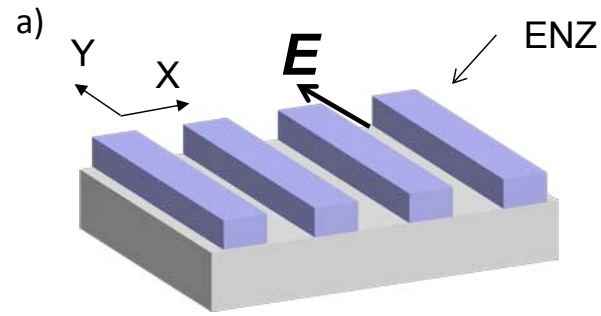

b)

Grat(%)	λ_{ENZ}(nm)	Trans
100	660	~0.1
70	690	~0.12
50	725	~0.17
30	800	~0.09

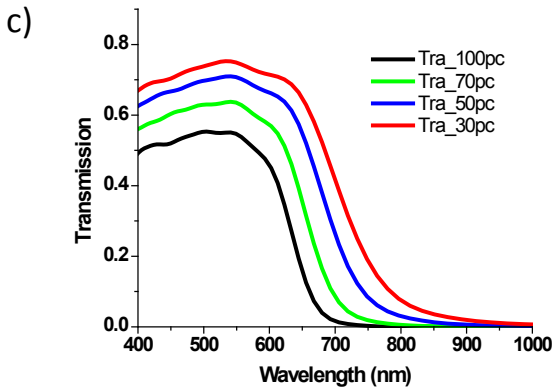

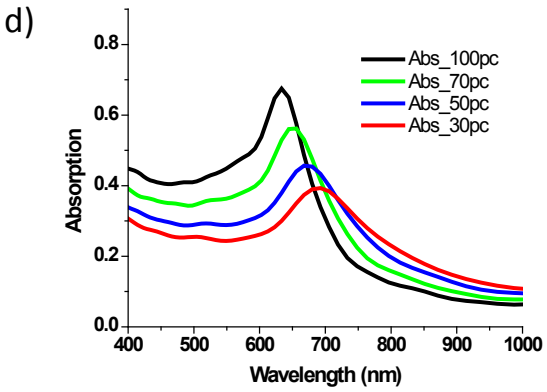

Figure 6: a) Schematic of the grating structure composed of ENZ material. b) Table showing grating size and t he corresponding ENZ wavelength and the associated transmission at that wavelength. c) FDTD transmission spectra for different grating percentages. d) the corresponding FDTD absorption spectra. T he grating period has been taken to be 100nm.

The field distribution across the grating is nearly uniform better approximating an effective medium. This structure thus opens the possibility of introducing emitters or gain medium in the gap region between the grating. It may be required that the refractive index of the gap region should not be changed significantly by the introduction of emitter medium. In this case, one can utilize spin coatable aerogel that can be functionalized with emitters to be introduced in the gap, a technique previously demonstrated for introducing quantum dot light emitters in photonic crystals[11].

Fabrication of 50nm wide gratings with a period of 100nm even for the 4pair structure turned out to be quite challenging. While electron beam direct patterning followed by etch would have provided a convenient approach, the resist thickness was insufficient as etch mask for a deep, large aspect ratio p attern transfer. We chose to use focused ion beam milling to fabricate the grating pattern ~ 20μm x 20μm in size (Figure 7a) b y further relaxing the lattice period (a) requirement to 250nm to minimize write time and to avoid problems associated with beam drift. The grating width was 160nm wider than anticipated due re-deposition during the milling process (Figure 7a rightside). We performed an FDTD simulation of this structure which consists of a 64% grating (Figure 7b). This like as is mentioned above shows increased transmission

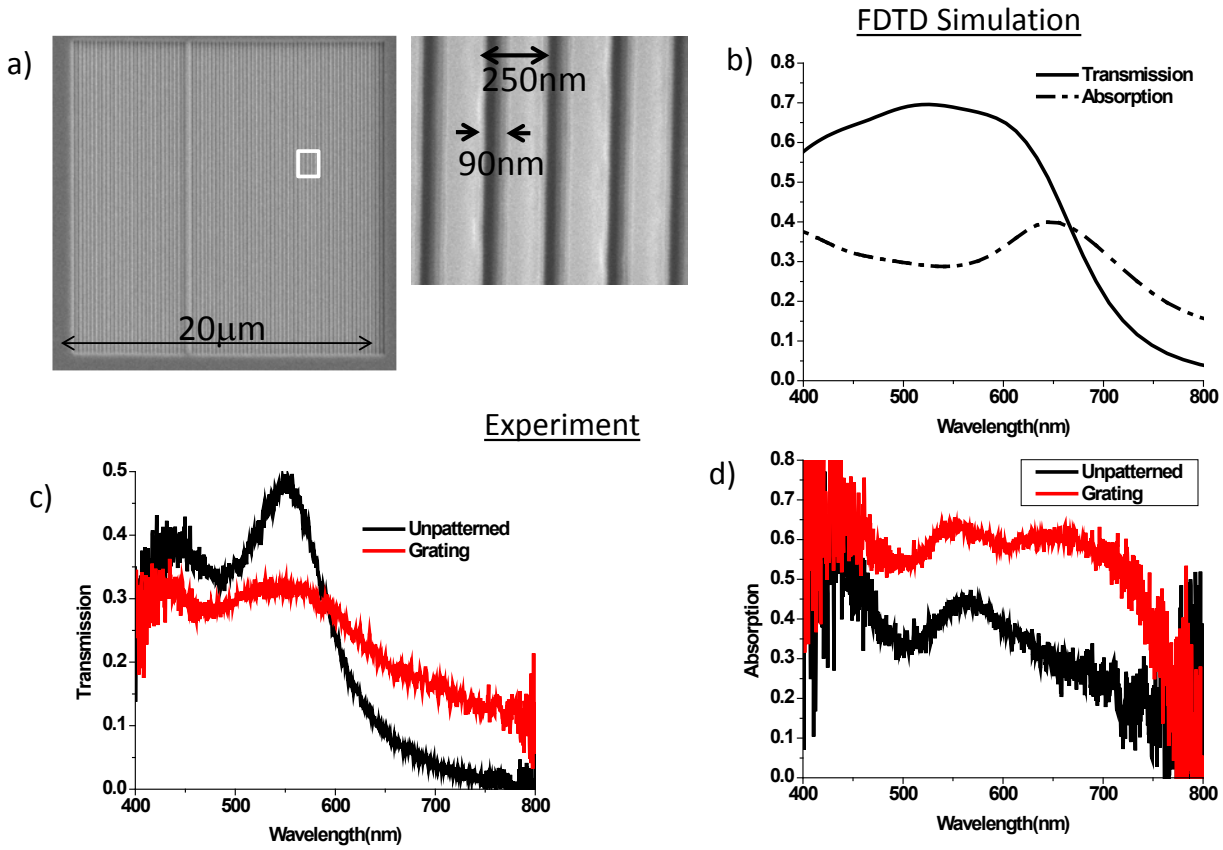

Figure 7: a)Top view SEM image of grating milled using focused ion beam on 4 layer ENZ structure. The right side image shows a magnified section in the square box. b) FDTD simulation of the fabricated structure showing transmission (solid) and absor ption (dashed). c) spectrum showing transmission from grating and unpatterned region. d) Corresponding absorption curves.

and reduced absorption. We measured optical transmission and reflection from the grating region with light polarized parallel to the grating using microspot spectroscopy system. Figure 7c, and d show the optical transmission and the absorption (calculated from A=1-T-R) measurements from the grating region as well as the nearby unpatterned region. The measured transmission shows a lower value than that from the unpatterned region below 600nm wavelength which is in contrast to what was expected from simulations. Nevertheless, we do observe a higher transmission from the grating beyond 600nm as expected from the simulations. Since the ENZ point shifts to a larger wavelength we still see an increased transmission for this region. The measured absorption is over 0.6 for most the measurement region. We believe this is likely due to incomplete or overmilling into the substrate as well as sidewall roughening resulting in scattering losses that reduces the transmission. A different fabrication approach such as aligned multilevel liftoff process that could provide smoother sidewalls would improve optical response and is currently under investigation. We have thus shown that an effective medium ENZ metamaterial with zero dielectric point in the visible can be fabricated using a metal-dielectric multilayer composite made from Ag and TiO_2.

A five layer structure shows the essential optical behavior of the ENZ structures and compares well with simulations. Choice of Ag/ TiO_2 is preferable over the Ag/ SiO_2 system as the former provides a smoother field distribution thus, better matching the effective medium response. Even with Ag's low imaginary part of dielectric constant at these wavelengths and its smaller fraction the multilayer composite still shows significant absorption. Creating a grating structure would potentially improve the transmission response while moving the ENZ point to longer wavelengths. The grating structure also opens up avenue for introducing active materials in the gaps enabling the possibility of loss control as well as light emission and absorption control.

3. BROADBAND NON-RESONANT LIGHT FUNNELING THROUGH ULTRA-SUBWAVELENGTH CHANNELS

In this section we describe a theoretical study of another approach that demonstrates ultra-subwavelength funneling of light that does not utilize ENZ metamaterial. This approach enables funneling of light to an area as small as $(\lambda/250)^2$ it across a substantially broad wavelength band. Current approaches to achieving light confinement and field enhancement typically involve the use of Extra-ordinary Optical Transmission (EOT) phenomena. This phenomenon was demonstrated for the first time in a thin silver film patterned with subwavelength sized cylindrical holes[12]. The phenomenon is so named because the transmitted light is beyond the expectations of Bethe's theory[13] and twice the amount predicted from a simple analysis based on the area fraction of the holes. The fundamental mechanism behind this behavior is due either to the excitation of surface plasmons[14] in the metal or dynamic diffraction or a combination of both. Nonetheless, they are resonant phenomena as a result, have unavoidably a narrow spectral bandwidth. A rectangular hole array etched into a thin Au film (~50nm) illustrates this further (Figure 8a). For a hole dimension of 100nm x 200 nm with a period of 'a' = 300nm a transmission as high as 0.8 is observed near 800 nm wavelength. The full width half maximum (FWHM) is approximately 250nm.The field distribution at this wavelength inside the rectangular hole shows an enhancement of 5X (Figure 8b).

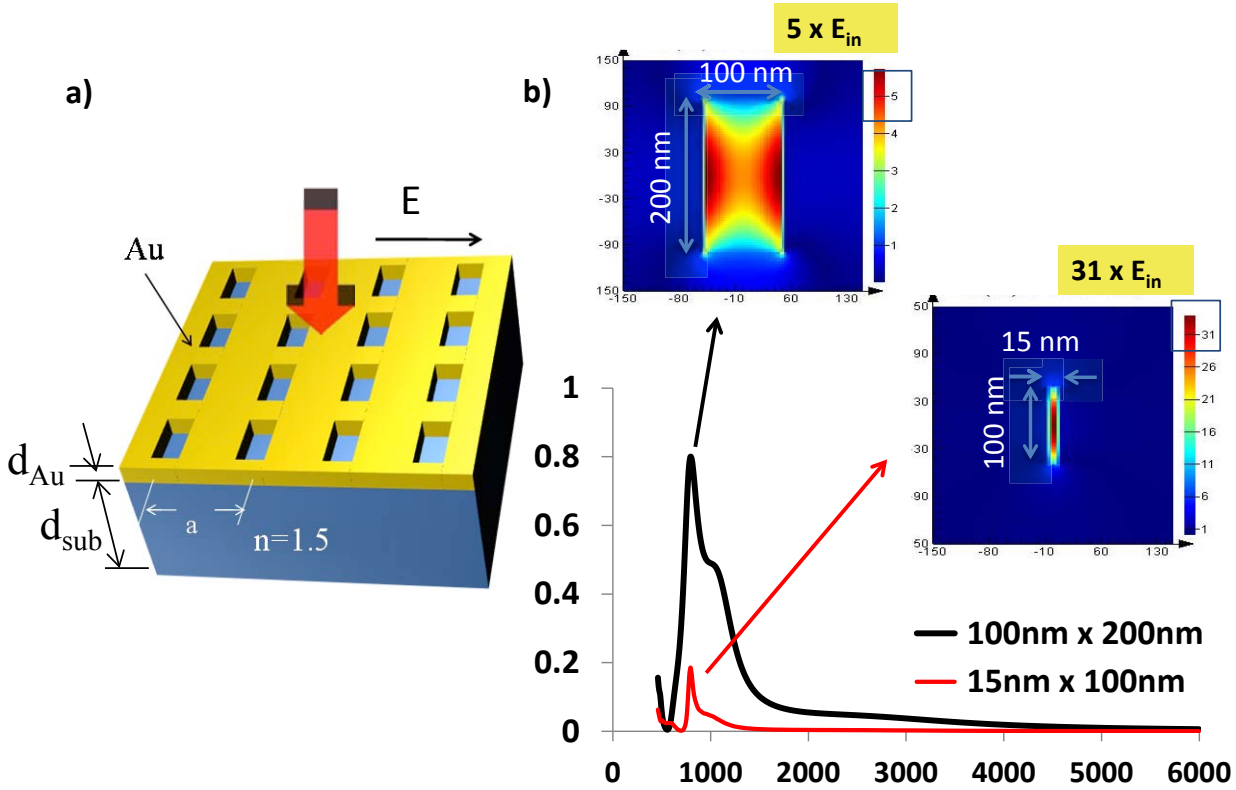

Figure 8:a) Schematic of a rectangular aperture array on Au thin film. b) Transmission response for two different hole dimension as well as the corresponding f ield distributions inside the hole.

The field enhancement can be increased to almost 30X (Figure 8b) by reducing the dimensions of the hole to 15 nm x 100 nm which however, comes at the expense of dramatically reducing the transmission down to ~ 0.2. The operational bandwidth can be increased by exploiting coupled resonances such as in nanoparticle dimers[15] or metallic slits that require fine tuning of the structural features, – size[15,16] shape[17,18] and/or angle of wave incidence[16].

It would be of great interest to explore the question if we can achieve light confinement and electric field enhancement while simultaneously achieving a broadband operation. One potential hint appears when we look at the optical response of a metallic grating structure (Figure 9a). Metallic gratings have high transmission (Figure 9b) across a large wavelength band for light polarized perpendicular to the grating orientation. However, the electric field enhancement is small (Figure 9c). The transmission is low for parallel polarized light hence such structures are typically used as highly efficient polarizer.

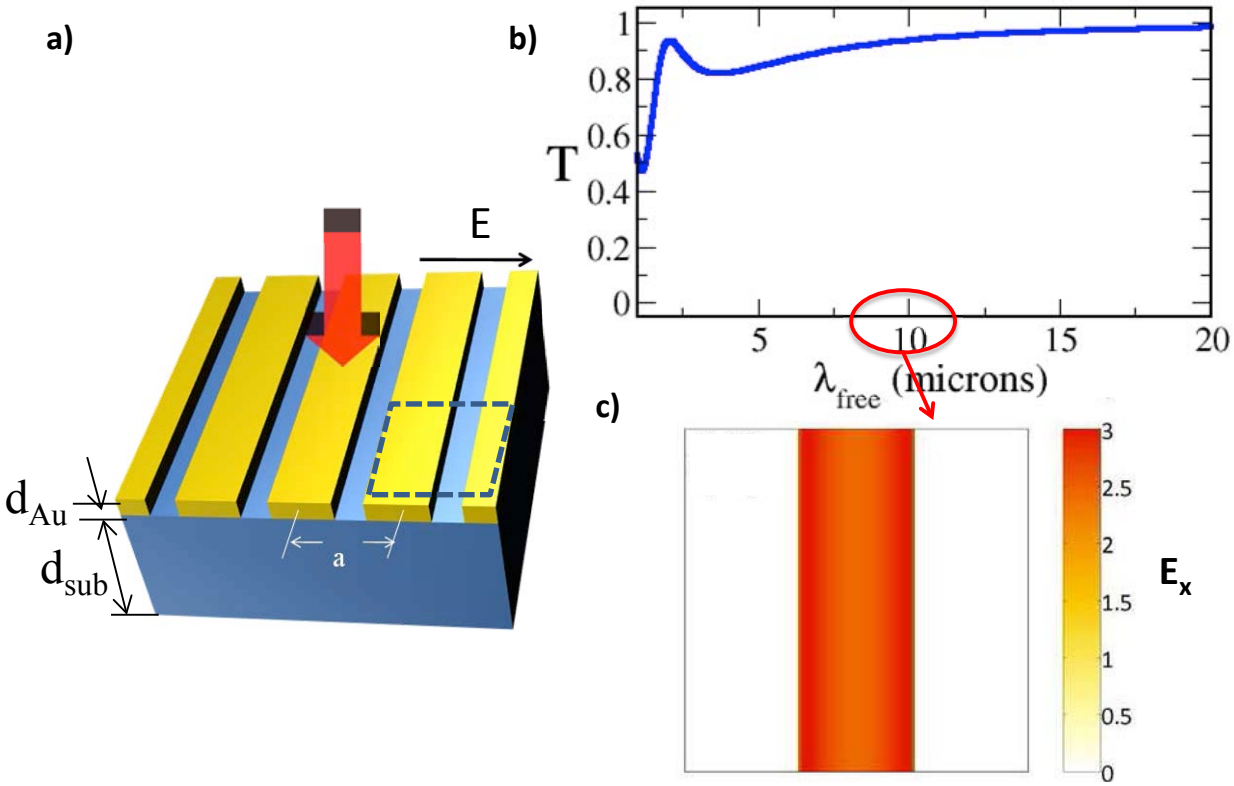

Figure 9:a) Schematic of a Au grating structure. b) Transmission response for light polarized perpendicular to the grating. c) Electric field in the gap between the metal lines.

Here we describe a paradigm structure which comprises of periodic connected rectangular apertures of two different sizes operating under normal incidence. This structure can be conceptualized as a combination of the rectangular hole array structure and the grating structure mentioned above (Figure 10a). The proposed structure is a square lattice of period a, consisting of alternating small and large rectangular slits engraved on a thin Au film of thickness d_{Au} resting on top a substrate of refractive index of n = 1.45 and thickness d_{sub} (Figure 10a). We study the optical transmission behavior for different combinations of w_{x1} and w_{x2}. In the limit of $w_{x1} = 0$ we obtain a rectangular hole structure. When $w_{x1}=w_{x2}$ we obtain a wire-grid (WG) structure. The

structure of interest is when neither $w_{x1}=w_{x2}$, nor $w_{x1} = 0$ which will be referred to as the double-groove (DG) structure.

To understand and explore the optical capabilities of the DG structure we study numerically the corresponding transmission spectrum between the wavelength range of 3 − 20μm. We employ the Finite Difference Time Domain (FDTD) approach[19], alongside with the Auxiliary Differential Equation (ADE)[15,19]method suitable for the modeling of the Drude dispersion (sec2, eq.1) for the permittivity [ε(ω)] in time domain[15] For comparison, we consider three different structures (one DG , one WG structure and one rectangular-hole structure). All are chosen to be deeply subwavelength to target the widest operation wavelength regime in the mid IR while being realistically achievable with nanofabrication methods.

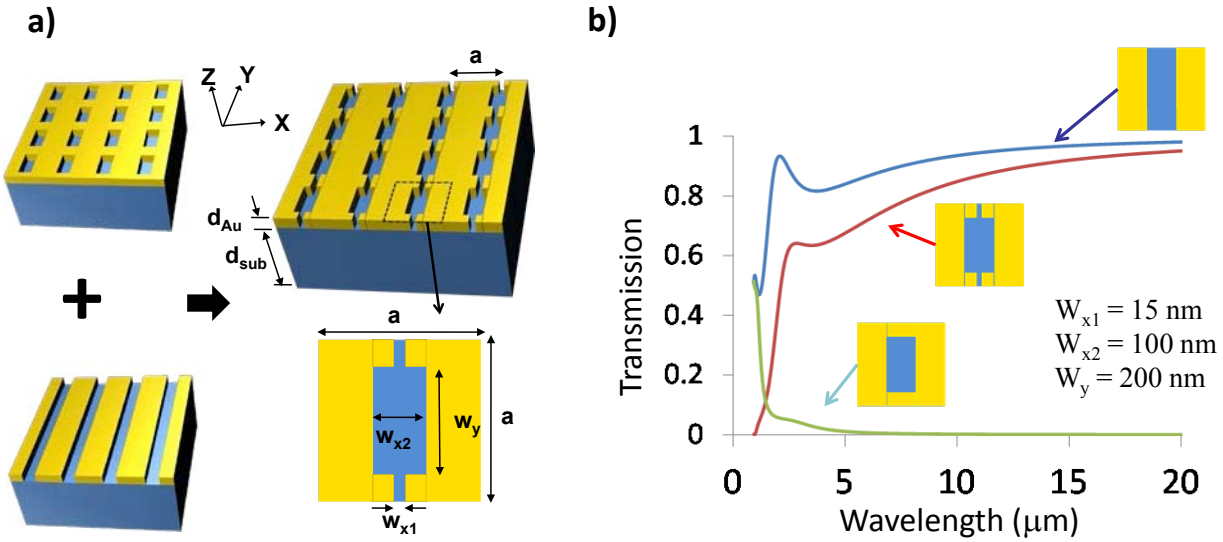

Figure 10:a) Schematic of the DG structure. b) Transmission plot for the nanohole, DG and the grating structure.

We show the simulation results for the transmission in (Figure 10b) versus the free space wavelength, λ_{free}, for a plane wave impinging the structure normally along the z-direction, with electric field polarized along the x-direction. All the considered structures have the following feature-size parameters common: a=300 nm, d_{Au} = 50nm, d_{sub}= 500nm, and w_y = 200 nm. We observe very low transmission for the rectangular structure (w_{x1} = 0 nm and w_{x2} = 100 nm) which is to be expected for a structure comprising of closed shaped apertures, for wavelengths above the EOT resonance. On the other end, for the grating structure (w_{x1} = 100 nm and w_{x2} = 100 nm) we notice a large transmission of over 0.8 from a wavelength of 3μm and larger. For the case of the DG structure (w_{x1} = 15 nm and w_{x2} = 100 nm) the tranmission behavior is quite similar to the grating structure but somewhat lower in magnitude. It is to be noted that the DG structure is geometrically closer to the rectangular hole array structure, nonetheless its transmission response is remarkably different. To further understand this behavior we look at the electric field distribution within the unit cell of the DG structure. We observe a highly enhanced field in the small-gap and a small field in the large-gap region. Also, the electric field remains nearly uniform in the small- and large-slit regions, except for a small fringing at the sharp interface between the two slits (Figure 11a). We also plotted the field intensity relative to the input field (E_0) for the large gap (E_L/ E_0) and the small gap (E_S /E_0) across the 3 − 20μm range.

The field ratio (E_L/ E_0) for the large gap varies (Figure 10b) from ~2 at the lower wavelength side and asymptotes to 3 for large wavelengths which is equal to the value (a/w_{x2}). Similarly for the
smaller gap (Figure 10c) the field ratio (E_S /E_0) goes from ~ 15 to ~ 20 at large wavelength which is equal to (a/w_{x1}).

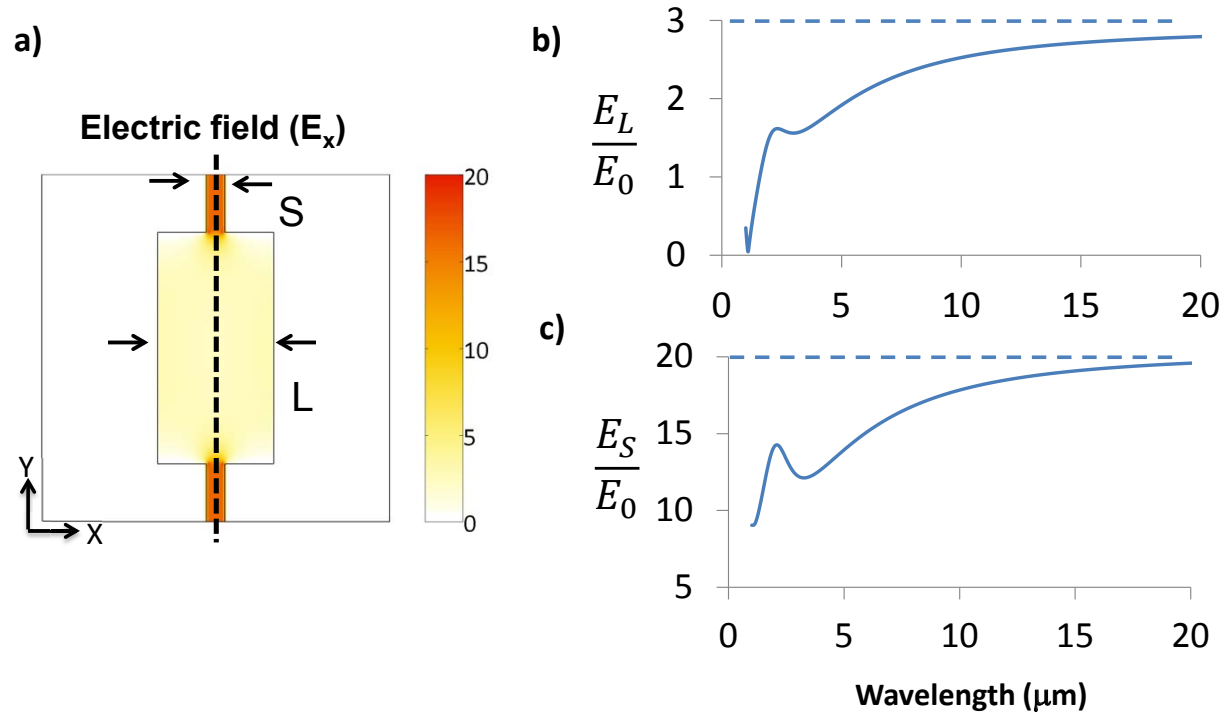

Figure 11:a) Electric field plot within the unit cell for λ = 10 μm. b) Electric field in the large gap as a function of wavelength. c) Electric field in the small gap as a function of wavelength.

Thus, if we plot the ratio of the electric field (Figure 12a) at the small gap to the large gap (E_L/ E_S) we find that it stays quite flat to about ~7 across the wavelength range that is of course, close to (w_{x2}/w_{x1}= 6.7). It turns out that this behavior can be explained well with a simple simple quasi-static picture wherein the electrons in the metal respond nearly instantaneously to the incident field. The charges build up across the gaps as depicted in the schematics (Figure 12b). As a result, the potential difference across the small slit, [points (1) and (2)] is equal to the potential difference across the large slit [points (3) and (4)]. This implies uniform electric field in each respective slit region with no phase difference and an amplitude ratio equal to the inverse of the ratio of the respective widths, as we have observed. In the long-wavelength regime, we can assume the structures are nearly transparent (i.e. almost zero reflection). We apply the continuity of the tangential component of the electric field at the interface, but averaged over the structural unit cell,and obtain:

$$\frac{E_L w_{x2} w_y + E_s w_{x1}(a - w_y)}{a^2} \quad \text{---(5)}$$

with E_0 being the source amplitude. Using in conjunction with the quasistatic condition for the

E_S/E_L ratio we get:

$$\frac{E_L}{E_0} \cong \frac{a}{w_{x2}} \quad \text{--- (6)}$$

and

$$\frac{E_S}{E_0} \cong \frac{a}{w_{x1}} \quad \text{---(7)}$$

We observe that this simple long-wavelength picture predicts the ratios E_L/E_0 and E_S/E_0 very well for both considered DG structures down to 10 micron wavelength below which it starts to deviate, nevertheless, remaining a reasonable estimate down to 3 μm.

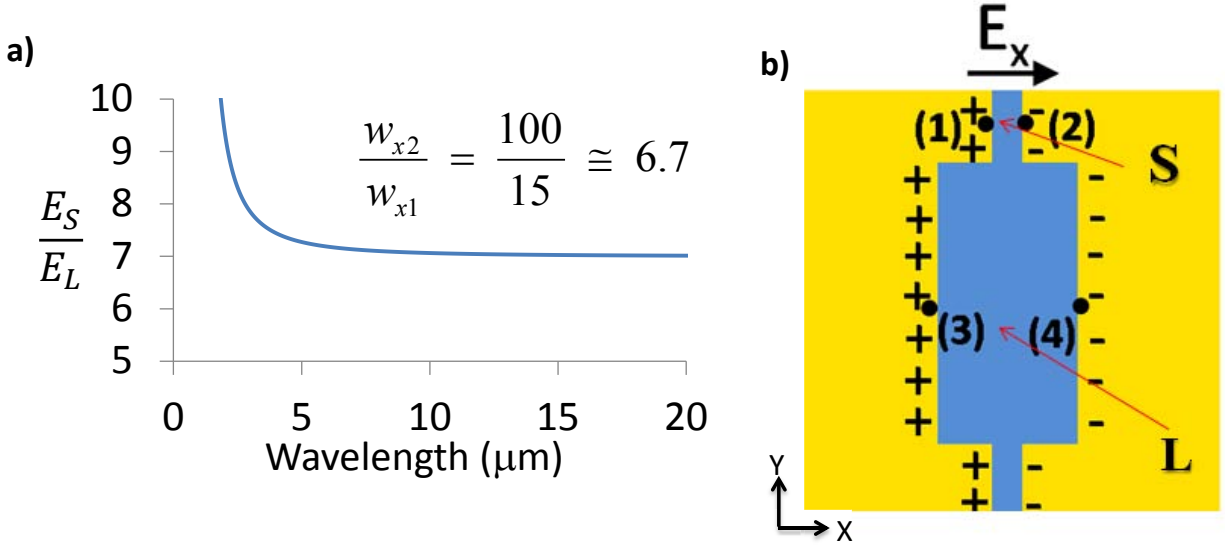

Figure 12:a) Ratio of electric field the small gap to the large gap. b) Schematic showing the quasitatic response of the charges in the metal within the DG unit cell.

Another point of interest is to determine how much power is carried through the small gap region via the highly confined enhanced electric field. To illustrate this let us consider the spatial distribution of the z-component of the Poynting vector (time-average value), S_z for the DG structure of w_{x1} = 15 nm, where we have an electric field enhancement factor of about 20 and confinement of the order of ~ $(\lambda/250)^2$ in the small slit area at 10 μm (Figure 13a). As expected almost no power is transmitted through the metallic region whilehaving a considerably larger power density in the small slit region compared to the large slit region. We calculate the integrated S_z in the small slit region, P_S, and the large slit region, P_L for the DG structure of Figure 13a within the unit cell. The respective areas of integration are designated in the figure. In Figure 13b we show the fraction of power that goes through the small slits, $F_{Ps} = P_S/(P_S + P_L)$, as a function of free space wavelength for such structure. We observe a large F_{Ps} of about 30% that remains nearly constant for the entire spectral region of interest. This is remarkable considering that the small slit region constitutes an area 60 times smaller than the unit cell area. At ~ 3μm wavelength, the structural periodicity effects start to emerge and we observe a sharp increase in F_{Ps} with the total transmission having decreased sharply. To quantify this behavior we find it

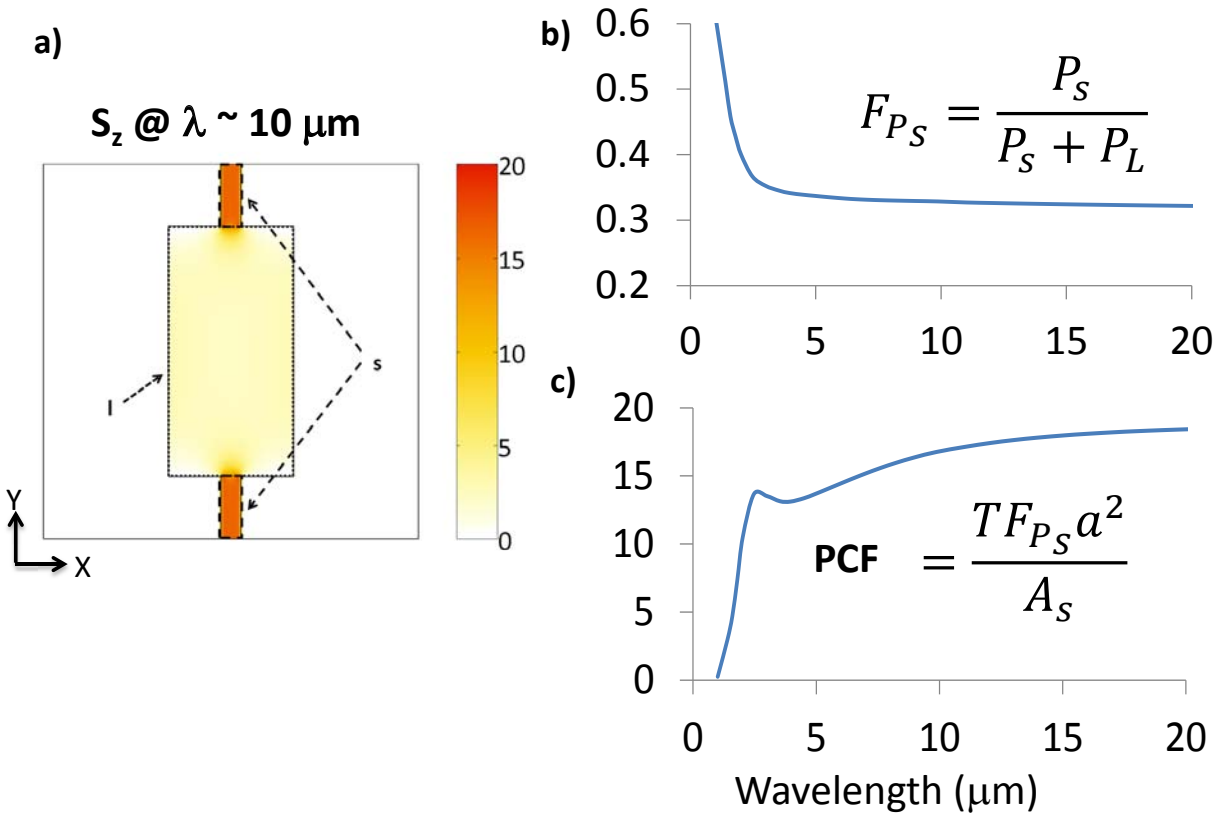

Figure 13:a) Poynting vector plot for the unit cell . b) Fraction of total power through the small gap. c) Power confinement factor (PCF) as a function of wavelength.

useful to introduce a figure-of-merit namely, the "Power Confinement Factor" (PCF) . We define PCF (Figure 13c)as the fraction of the incident power that gets funneled through the small slit region divided by the area fraction covered by the small slit region, i.e. PCF = T $F_{Ps}a^2/A_s$, with A_s being the area covered by the small grooves within the unit cell. PCF is analogous to the transmission enhancement factor which serves as a figure-of-merit in resonant EOT platforms .

These results show an alternative approach to achieving subwavlength light control that does not require ENZ. It provides a counterexample to the widespread and intuitive notion that resonances are needed to funnel light with enhanced intensity through deep subwavelength apertures. The double-groove structure described above effectively combines the broadband transmission property of a one-dimensional grating with the field confinement and enhancement properties of subwavelength apertures. The structure thus possesses the attractive features of EOT platforms, while being non-resonant and broadband.

4. SUMMARY AND FUTURE WORK

Over the course of this Early Career LDRD we have explored ENZ metamaterials in the visible regime. We developed a process and fabricated a metal-dielectric multilayer composite structure to achieve ENZ at a wavelength of ~ 660nm. The structure was composed of 16nm thick Ag and 54nm thick TiO_2 deposited in a layer by layer fashion using electron beam evaporation. Transmission response measured on different number of layers indicated that the effect of losses arising from the metal component albeit being chosen for the reason having intrinsically low absorption in the visible, was quite significant. Creating of one-dimensional gratings on these structures appear to somewhat mitigate this problem but the transmission at the ENZ wavelengths remain low (< 0.2). There is however, improved transmission at wavelengths smaller than the ENZ wavelength but where the effective still less than unity. This is an interesting regime and can be further explored for light confinement in air. Also, the creation of gratings enables introduction of active materials that can be utilized to combat the loss effects. However, this will require fabrication of deep gratings with nanometer scale widths in order to achieve field uniformity and thus, poses a significant fabrication challenge that needs be addressed. Other potential approaches could involve replacing Ag with graphene. This LDRD enabled a CINT user proposal providing effective utilization of the CINT and Microfabricaton facilities for fabrication.

While investigating the ENZ approach to sub-wavelength light control, we also explored alternative approaches theoretically. This led to the discovery of the double-groove (DG), metal structures for achieveing a broad band ultra-subwavelength [$\sim (\lambda/250)^2$] light confinement with large electric field enhancement (~ 20X). The structure essentially consists of a series of alternating small and large rectangular slits etched into a thin gold film that lies on a dielectric substrate. A non-resonant mechanism where the electrons respond nearly instantaneously to the incident field enables the trapping of the electromagnetic field into the groove structure. This work was the result of a collaborative effort with a CINT visitor, Dr. S. Foteinopoulou of University of Exeter, UK . The next step in this effort is the fabrication and optical testing of these structures. Due to nanometerscale dimensions and large area requirments of the structure the fabrication poses considerable challenges. Nonetheless, towards the end of this LDRD we have been able to achieve some success toward the fabrication of these structures.

5. REFERENCES

1. Silveirinha, M. & Engheta, N. Tunneling of Electromagnetic Energy through Subwavelength Channels and Bends using epsilon -Near-Zero Materials. *Phys. Rev. Lett.* **97**, 157403 (2006).
2. Pan, Y. & Xu, S. Energy tunnelling through an ultrasmall epsilon-near-zero channel in circular waveguide. *Microwaves, Antennas & Propagation, IET* **3**, 821-825 (2009).
3. Edwards, B., Alù, A., Young, M. E., Silveirinha, M. & Engheta, N. Experimental Verification of Epsilon-Near-Zero Metamaterial Coupling and Energy Squeezing Using a Microwave Waveguide. *Phys. Rev. Lett.* **100**, 033903 (2008).
4. Alù, A. & Engheta, N. All Optical Metamaterial Circuit Board at the Nanoscale. *Phys. Rev. Lett.* **103**, 143902 (2009).
5. Cai, W. & Shalaev, V. *Optical Metamaterials: Fundamentals and Applications* 1st edn, (Springer, 2010).
6. Nielsen, R. *et al.* Toward superlensing with metal–dielectric composites and multilayers. *Applied Physics B: Lasers and Optics* **100**, 93-100, doi:10.1007/s00340-010-4065-z (2010).
7. Pollard, R. J. *et al.* Optical Nonlocalities and Additional Waves in Epsilon-Near-Zero Metamaterials. *Phys. Rev. Lett.* **102**, 127405 (2009).
8. Ramakrishna, S. A., Pendry, J. B., Wiltshire, M. C. K. & Stewart, W. J. Imaging the near field. *Journal of Modern Optics* **50**, 1419-1430 (2003).
9. Ramakrishna, S. A., Pendry, J. B., Wiltshire, M. C. K. & Stewart, W. J. Imaging the near field. *Journal of Modern Optics* **50**, 1419 - 1430 (2003).
10. Palik, E. D. (Academic Press, 1985).
11. Subramania, G. *et al.* Emission modification of CdSe quantum dots by titanium dioxide visible logpile photonic crystal. *Applied Physics Letters* **95**, 151101-151103 (2009).
12. Ebbesen, T. W., Lezec, H. J., Ghaemi, H. F., Thio, T. & Wolff, P. A. Extraordinary optical transmission through sub-wavelength hole arrays. *Nature* **391**, 667-669 (1998).
13. Bethe, H. A. Theory of Diffraction by Small Holes. *Physical Review* **66**, 163 (1944).
14. Ghaemi, H. F., Thio, T., Grupp, D. E., Ebbesen, T. W. & Lezec, H. J. Surface plasmons enhance optical transmission through subwavelength holes. *Physical Review B* **58**, 6779 (1998).
15. Foteinopoulou, S., Vigneron, J. P. & Vandenbem, C. Optical near-field excitations on plasmonic nanoparticle-based structures. *Opt. Express* **15**, 4253-4267 (2007).
16. Huang, X.-R., Peng, R.-W. & Fan, R.-H. Making Metals Transparent for White Light by Spoof Surface Plasmons. *Phys. Rev. Lett.* **105**, 243901 (2010).
17. Matteo, J. *et al.* Spectral analysis of strongly enhanced visible light transmission through single C-shaped nanoapertures. *Applied Physics Letters* **85**, 648 (2004).
18. Shi, X., Hesselink, L. & Thornton, R. L. Ultrahigh light transmission through a C-shaped nanoaperture. *Opt. Lett.* **28**, 1320-1322 (2003).
19. Hagness, A. T. a. S. C. *Computational Electrodynamics: The Finite-Difference Time-Domain Method*. 3rd edn, (Artech House, 2005).

APPENDIX A: LIST OF PUBLICATIONS AND PRESENTATIONS

Publications

1. G.Subramania, S.Foteinopoulou and I. Brener, *"Non-resonant broadband squeezing of light via ultra-subwavelength channels"- Phys. Rev. Lett. 107, 163902 (2011)*
2. .G.Subramania and Art Fischer , *"Optical properties of metal-dielectric multilayer based Epsilon Near Zero metamaterial "*, in preparation.

Presentations

1. G.Subramania and Art Fischer,*" ENZ behavior of Ag/TiO2 multilayer composites"*, Presentation MRS Fall 2011, Boston. (oral)
2. G.Subramania, S.Foteinopoulou and I. Brener, *"Non-resonant broadband squeezing of light via ultra-subwavelength channels",*APS March meeting ,2012, Boston. (oral)
3. G.Subramania, S.Foteinopoulou and I. Brener, *"Non-resonant broadband squeezing of light via ultra-subwavelength channels", PECS-X conference, Santa Fe, NM, June 2012.* (poster)
4. G.Subramania, S.Foteinopoulou and I. Brener, *"Non-resonant broadband squeezing of light via ultra-subwavelength channels", Trilab Symposium, Washington DC, June 2012.* (poster)

Special Mentions and Press

1. G.Subramania et.al. " Synopsis: Light Gets into the Double Groove", Editor synopsis, Phys. Rev. Lett. Oct 2011. (http://physics.aps.org/synopsis-for/10.1103/PhysRevLett.107.163902)
2. G.Subramania et. al. "New way to funnel light could have infrared applications" Physorg. Com Oct 2011 (http://www.physorg.com/news/2011-10-funnel-infrared-applications.html).
3. "Nonresonant Broadband Funneling of Light via Ultrasubwavelength Channels," LDRD Monthly News report brief, March 2012.

DISTRIBUTION

1	MS1304	Ting S. Luk	1131
1	MS1421	Jerry A. Simmons	1120
1	MS1421	J. Charles Barbour	1100
1	MS1078	Wahid L. Hermina	1710
1	MS1082	Ganapathi S. Subramania	1126
1	MS1082	Igal Brener	1727
1	MS1086	Arthur J. Fischer	1123
1	MS1086	Robert M. Biefeld	1126
1	MS0899	Technical Library	9536 (electronic copy)
1	MS0359	D. Chavez, LDRD Office	1911


Sandia National Laboratories